Mem. S.A.It. Vol. 94, 99

Memorie della

CERES survey

Stellar parameters and chemical abundances of selected elements

L. Lombardo[1]

GEPI, Observatoire de Paris, Université PSL, CNRS, 5 place Jules Janssen 92195 Meudon, France
e-mail: Linda.Lombardo@observatoiredeparis.psl.eu

Received: 16-11-2022; Accepted: 08-12-2022

Abstract. The Chemical Evolution of R-process Elements in Stars (CERES) project has the aim to obtain a complete chemical inventory of a sample of 52 halo giant stars with metallicities below −1.5, in order to understand the physical conditions and formation scenarios of neutron capture elements. To achieve this, we rely on a sample of high resolution and high signal-to-noise ratio spectra obtained with UVES at the ESO/VLT. We measured chemical abundances of 26 species of 18 elements (Na, Mg, Al, Si, Ca, Sc, Ti, V, Cr, Mn, Fe, Co, Ni, Cu, Zn, Sr, Y, and Zr). The homogeneity of the analysis allowed us to detect the presence in the sample of two stars with [Zn/Fe]∼+0.7, one r-rich and the other r-poor. This suggests that the Zn enrichment is not produced by the r-process in both stars. We identified two branches in the [Zn/Fe] versus [Ni/Fe] diagram. We suggest that the high [Zn/Fe] branch is the result of hypernova nucleosynthesis. We found several stars with peculiar light neutron-capture abundance patterns. In particular, CES1237+1922 (also known as BS 16085-0050), which shows Sr, Y, and Zr values ∼1 dex lower than other stars in the sample.

Key words. Galaxy: abundances – Galaxy: evolution – Stars: abundances – Stars: Population II – Stars: Population III – Nuclear reactions, nucleosynthesis, abundances

1. Introduction

Elements beyond the iron-peak ($Z > 30$) are called neutron-capture (n-capture) elements, since the most efficient way to produce them is by neutron captures on a seed nucleus, usually an iron-peak element. A neutron capture creates a nucleus far from the stability valley, and the system tries to fall back to the valley through β decays. Neutron captures can be distinguished in three distinct processes, depending on the neutron flux. At neutron densities below $\sim 10^8$ cm^{-3}, the timescale between two consecutive neutron captures is less than that of β decay (see e.g. Busso et al. 1999, and references therein). This process is called slow neutron capture, or *s*-process. When the neutron flux is so high that the seed nucleus can capture several neutrons before decaying, at densities above 10^{24} cm^{-3}, the process is called rapid neutron capture, or *r*-process (see e.g. Kratz et al. 2007, and references therein).

In the intermediate neutron density range, between 10^{14} cm^{-3} and 10^{16} cm^{-3}, we refer to the intermediate neutron capture process, or *i*-process (Cowan & Rose 1977).

Observationally, metal-poor stars show a broad range of n-capture abundance patterns, with a large scatter of the abundance ratios as a function of metallicity (McWilliam et al. 1995; Burris et al. 2000; François et al. 2007; Hansen et al. 2012), in contrast to the very tight relation with [Fe/H] shown by lighter elements (McWilliam et al. 1995; Cayrel et al. 2004; Bonifacio et al. 2009). This evidence seems to suggest that the n-capture elements are produced in different formation sites and under different physical conditions, at variance with the lighter elements, which are formed in hydrostatic or explosive burning in Type II and Type Ia supernovae (SNe) (see e.g. Arnett 1996).

As extensively discussed in the recent review by Cowan et al. (2021), neutron densities high enough to allow the *r*-process can be reached in different environments, for example in neutrino winds from core-collapse supernovae, in electron-capture supernovae, in magneto-rotational supernovae, and in the mergers between two neutron stars or between a neutron star and a black hole. The recent identification of strontium in the merger of two neutron stars by Watson et al. (2019) demonstrates that the *r*-process does occur in neutron-star mergers. However, it is still unclear whether other formation sites exist, and under which physical conditions the various n-capture elements can be formed, particularly at low metallicities (see e.g. Qian & Wasserburg 2001, 2007; Hansen et al. 2014; Spite et al. 2018; Skúladóttir & Salvadori 2020; and the reviews by Sneden et al. 2008; Cowan et al. 2021).

The Chemical Evolution of R-process Elements in Stars (CERES) project has the objective of providing detailed chemical abundances, in particular of n-capture elements, in a sample of 52 giant stars with [Fe/H] < -1.5, in order to test different theoretical scenarios for n-capture processes. In this study we performed a homogeneous analysis of a set of high resolution (R > 40000) and high signal-to-noise ratio (S/N) spectra (S/N between 50 and 120 per pixel at 390 nm) observed with UVES at ESO/VLT (Dekker et al. 2000) .

2. Chemical analysis

2.1. Stellar parameters

We derived the stellar parameters using Gaia Early Data Release 3 (EDR3) photometry and parallaxes (Gaia Collaboration et al. 2016, 2021). The effective temperatures ($T_{\rm eff}$) and surface gravities (log g) for our sample of stars have been derived using the iterative procedure shown in Fig. 1. The procedure is based on a grid, defined in the parameters space, which contains theoretical values of $G_{BP} - G_{RP}$, bolometric correction (BC_G), extinction coefficients A_G, and the reddening E($G_{BP} - G_{RP}$), for each set of $T_{\rm eff}$, log g, and [Fe/H]. Synthetic colours and extinction coefficients are calculated using grids of ATLAS 9 1D plane-parallel model atmosphere by Castelli & Kurucz (2003). The reddening E($G_{BP} - G_{RP}$) is computed using the reddening law of Fitzpatrick et al. (2019). The grid is defined in the range of parameters $3500 \leq T_{\rm eff} \leq 6000$ K, $0 \leq \log g \leq 4$ dex, and $-4 \leq$ [Fe/H] $\leq +0.5$. The α-elements are enhanced by +0.4 dex for all models with [Fe/H] ≤ -1, and they are solar-scaled for higher metallicity models. To derive the stellar parameters the procedure needs the Gaia photometry (G, $G_{BP} - G_{RP}$) and parallax, the reddening E($B-V$), and the metallicity of the star. The reddening values E($B-V$) are taken from the reddening maps by Schlafly & Finkbeiner (2011, $A_V = 0.81$) At the beginning of the first run, [Fe/H] is fixed at the input value, log g is fixed at 2.0 dex, and the reddening is assumed to be zero. Since the sample stars are giants, a 0.8 M$_\odot$ mass is assumed. The procedure derives the $T_{\rm eff}$ and log g in different steps, and it is repeated until the difference in log g between consecutive runs is smaller than 0.05 dex and the difference in $T_{\rm eff}$ is less than 50 K. The iron abundance is then derived using MyGIsFOS with the new set of stellar parameters, and the procedure is repeated with the newly found [Fe/H] as input. If the difference between the new and the old $T_{\rm eff}$ is

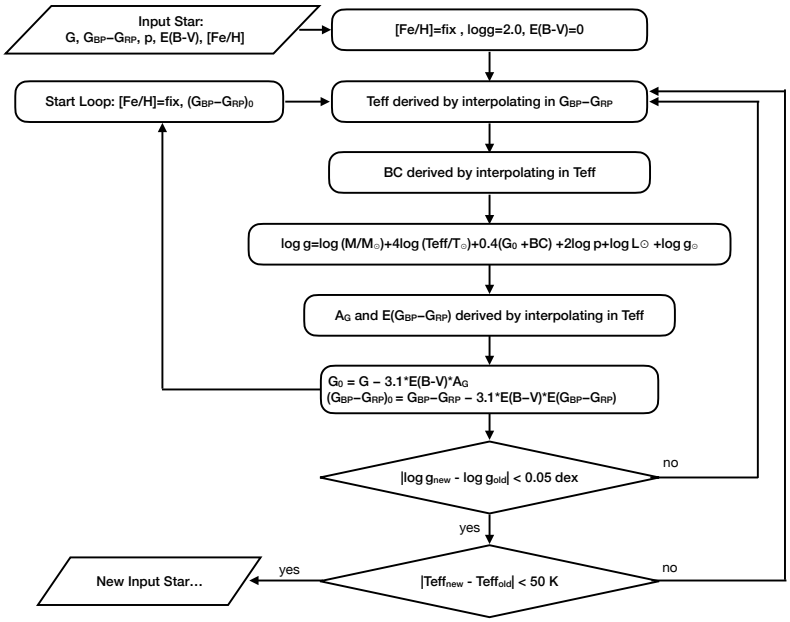

Fig. 1. Diagram of the iterative procedure employed to derive the stellar parameters.

more than 50 K, we derive again [Fe/H], and the procedure is repeated until the parameters converge. The convergence is usually reached after two iterations. Microturbulent velocities (v_{turb}) were estimated using the calibration derived by Mashonkina et al. (2017). The stellar parameters we derived are listed in Table 1 in Lombardo et al. (2022). With this choice of parameters, we find a mean difference between [FeII/H] and [FeI/H] of 0.13, with σ = 0.09. The other names and coordinates for the targets are provided in Table A.1 of Lombardo et al. (2022).

2.2. Chemical abundances

The chemical abundances of 26 species of 18 elements (Na, Mg, Al, Si, Ca, Sc, Ti, V, Cr, Mn, Fe, Co, Ni, Zn, Sr, Y and Zr) were derived for the sample stars using MyGIsFOS (Sbordone et al. 2014). Thanks to the high quality of our spectra, we could measure the abundances of hardly detectable ions, such as Si II, Sc I, Mn II, and Zr I. The derived chemical abundances are only available at the CDS via anonymous ftp to `cdsarc.u-strasbg.fr` (`ftp://130.79.128.5`) or via `http://cdsarc.u-strasbg.fr/viz-bin/cat/J/A+A/665/A10`.

In general, our derived chemical abundances are in good agreement with the literature values for halo stars, particularly when compared with those obtained by Cayrel et al. (2004), Ishigaki et al. (2012, 2013), and Cescutti et al. (2022, A&A, accepted; hereafter MINCE). However, we note that both our and MINCE Cr abundances show some discrepancies with Cayrel et al. (2004) and Ishigaki et al. (2013), as shown in Fig. 2. In our study and in MINCE, Cr I and Cr II were derived using MyGIsFOS adopting the same list of Cr lines. The first difference consists in an offset between our and MINCE abundance ratios and

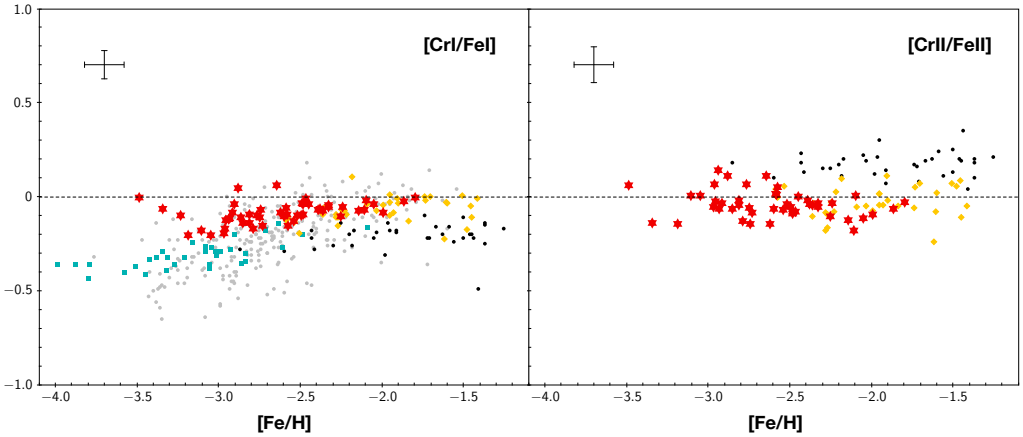

Fig. 2. [Cr I/Fe I] and [Cr II/Fe II] as a function of [Fe/H] for stars in our sample (red star symbols). Cyan squares, black dots, yellow diamonds, and grey dots represent the same quantities for stars of similar metallicity in Cayrel et al. (2004), in Ishigaki et al. (2013), in Cescutti et al. (2022, A&A, accepted), and in Barklem et al. (2005) respectively. A representative error is plotted in the upper-left corner of each panel.

those in Cayrel et al. (2004) and Ishigaki et al. (2013). We find that our [Cr I/Fe I] abundance ratios are on average ∼ 0.15 dex higher than Cayrel et al. (2004) and Ishigaki et al. (2013), and the [Cr II/Fe II] abundance ratios are on average ∼ 0.2 dex lower than Ishigaki et al. (2013) values. The second difference concerns the trend of [Cr I/Fe I] abundance ratios as a function of the metallicity. Both in Cayrel et al. (2004) and Ishigaki et al. (2013), a decreasing trend with metallicity is observed. In our and MINCE samples instead, there is no trend down to [Fe/H] = −2.5. Then [Cr I/Fe I] decreases to reach a minimum for [Fe/H] = −3.0. For lower metallicities we can guess an increase but we have too few data to state a firm conclusion. Another important difference that we observe is that, in our and MINCE samples, both [Cr I/Fe I] and [Cr II/Fe II] are close to zero, with [Cr I/Fe I]=−0.09 (σ = 0.06) and [Cr II/Fe II]=−0.04 (σ = 0.07), which is theoretically expected since Cr and Fe are both formed under the same physical conditions. We attribute these discrepancies to the different linelists, since previous investigations, as in Cayrel et al. (2004), relied mostly on Cr I resonance lines, which are strongly affected by non-local thermodynamic equilibrium (NLTE) effects. Apparently, the Cr I lines we chose for the analysis seem to be less affected by NLTE, which explains why we do not observe any trend with metallicity, but, instead, we observe the ionisation balance between Cr I and Cr II.

The analysis revealed the presence of two stars with Zn abundances much higher than the average ([Zn/Fe]∼+0.7): CES1543+0201, also known as CS 30312–100, and CES2254-4209, also known as HE2252-4225. Most intriguingly, the two stars appear to have different enrichment histories, since CES1543+0201 is r-poor ([Eu/Fe]=–0.2, Roederer et al. 2014) and CES2254–4209 is r-rich ([*r*/Fe]=+0.8, Mashonkina et al. 2014). The conclusion is that in the r-poor star, Zn was created by a nucleosynthesis path other than the r-process.

Following the study of Skúladóttir et al. (2017) about Zn abundance in red giant branch stars of the Sculptor dwarf galaxy, we found a correlation between Zn and Ni abundances in our sample. In particular, we note that the stars appear to follow two different branches in the [Zn/Fe] versus [Ni/Fe] plot, as shown in Fig. 3. We think that these two branches could be due to differences in the explosion energies of supernovae (SNe) depending on the mass of the progenitor star (see e.g. Nomoto et al.

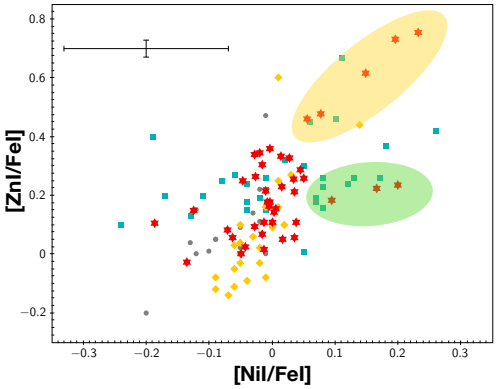

Fig. 3. [Zn/Fe] as a function of [Ni/Fe] for stars in our sample (red star symbols). Other symbols are the same as in Fig. 2 for stars in the same metallicity range of our sample stars. A representative error is plotted in the upper-left corner.

2013, and references therein). Hypernova explosions ($E_{kin} \geq 10^{52}$ erg) can produce larger amount of iron-peak elements, particularly Zn, than classical core-collapse SNe through α-rich freeze-out process (see e.g. Galama et al. 1998; Iwamoto et al. 1998; Nomoto et al. 2001; Umeda & Nomoto 2002). Therefore, it is possible that the stars along the high Zn branch formed in a gas cloud enriched by hypernovae, while the stars with normal Zn formed from gas enriched by classic SNe.

The analysis also revealed that six stars in the sample have peculiar light n-capture element abundance patterns:

- CES1237+1922 (also known as BS 16085-0050) is deficient in Sr, Y and Zr compared to stars of similar metallicity, with [Sr II/Fe II]=−1.66, [Y II/Fe II]=−1.21, and [Zr II/Fe II]=−1.04.
- CES0109-0443 (also known as CS 22183-031) is underabundant in Sr with respect to Y and Zr, with [Y II/Sr II]=+0.34 and [Zr II/Sr II]=+0.59.
- CES2250-4057 (also known as CD-41 15048, also known as HE 2247-4113) is overabundant in Sr with respect to Y and Zr, with [Y II/Sr II]=−0.80 and [Zr II/Sr II]=−0.46.
- CES1322-1355 (also known as HE 1320-1339), is overabundant in Sr with respect to Y and Zr, with [Y II/Sr II]=−0.55 and [Zr II/Sr II]=−0.33.
- CES0547-1739 (also known as TYC 5922-517-1) is overabundant in Zr with respect to Sr and Y, with [Zr II/Sr II]=+0.68 and [Zr II/Y II]=+0.70.
- CES0424-1501 (also known as BD-15 779) is overabundant in Zr with respect to Sr and Y, with [Zr II/Sr II]=+0.54 and [Zr II/Y II]=+0.62.

3. Conclusions

The homogeneous analysis we performed allowed us to highlight many chemical peculiarities in our sample stars. Stellar parameters derived in this study will be used to determine other heavy n-capture element abundances in future papers of the CERES project. When a complete chemical inventory for these stars will be available, it will allow us to draw further conclusions on the formation scenarios and the possible formation channels of these elements.

Acknowledgements. I gratefully acknowledge support from the French National Research Agency (ANR) funded project “Pristine” (ANR-18- CE31-0017). This project has received funding from the European Research Council (ERC) under the European Union’s Horizon 2020 research and innovation programme (grant agreement No. 804240). This work has made use of data from the European Space Agency (ESA) mission *Gaia* (`https://www.cosmos.esa.int/gaia`), processed by the *Gaia* Data Processing and Analysis Consortium (DPAC, `https://www.cosmos.esa.int/web/gaia/dpac/consortium`). Funding for the DPAC has been provided by national institutions, in particular the institutions participating in the *Gaia* Multilateral Agreement. This article is based upon work from the “ChETEC” COST Action (CA16117), supported by COST (European Cooperation in Science and Technology).

References

Arnett, D. 1996, Supernovae and Nucleosynthesis: An Investigation of

the History of Matter from the Big Bang to the Present
Barklem, P. S., Christlieb, N., Beers, T. C., et al. 2005, A&A, 439, 129
Bonifacio, P., Spite, M., Cayrel, R., et al. 2009, A&A, 501, 519
Burris, D. L., Pilachowski, C. A., Armandroff, T. E., et al. 2000, ApJ, 544, 302
Busso, M., Gallino, R., & Wasserburg, G. J. 1999, ARA&A, 37, 239
Castelli, F. & Kurucz, R. L. 2003, in IAU Symposium, Vol. 210, Modelling of Stellar Atmospheres, ed. N. Piskunov, W. W. Weiss, & D. F. Gray, A20
Cayrel, R., Depagne, E., Spite, M., et al. 2004, A&A, 416, 1117
Cowan, J. J. & Rose, W. K. 1977, ApJ, 212, 149
Cowan, J. J., Sneden, C., Lawler, J. E., et al. 2021, Reviews of Modern Physics, 93, 015002
Dekker, H., D'Odorico, S., Kaufer, A., Delabre, B., & Kotzlowski, H. 2000, in Society of Photo-Optical Instrumentation Engineers (SPIE) Conference Series, Vol. 4008, Optical and IR Telescope Instrumentation and Detectors, ed. M. Iye & A. F. Moorwood, 534–545
Fitzpatrick, E. L., Massa, D., Gordon, K. D., Bohlin, R., & Clayton, G. C. 2019, ApJ, 886, 108
François, P., Depagne, E., Hill, V., et al. 2007, A&A, 476, 935
Gaia Collaboration, Brown, A. G. A., Vallenari, A., et al. 2021, A&A, 649, A1
Gaia Collaboration, Prusti, T., de Bruijne, J. H. J., et al. 2016, A&A, 595, A1
Galama, T. J., Vreeswijk, P. M., van Paradijs, J., et al. 1998, Nature, 395, 670
Hansen, C. J., Montes, F., & Arcones, A. 2014, ApJ, 797, 123
Hansen, C. J., Primas, F., Hartman, H., et al. 2012, A&A, 545, A31
Ishigaki, M. N., Aoki, W., & Chiba, M. 2013, ApJ, 771, 67
Ishigaki, M. N., Chiba, M., & Aoki, W. 2012, ApJ, 753, 64
Iwamoto, K., Mazzali, P. A., Nomoto, K., et al. 1998, Nature, 395, 672
Kratz, K.-L., Farouqi, K., Pfeiffer, B., et al. 2007, ApJ, 662, 39
Lombardo, L., Bonifacio, P., François, P., et al. 2022, A&A, 665, A10
Mashonkina, L., Christlieb, N., & Eriksson, K. 2014, A&A, 569, A43
Mashonkina, L., Jablonka, P., Pakhomov, Y., Sitnova, T., & North, P. 2017, A&A, 604, A129
McWilliam, A., Preston, G. W., Sneden, C., & Searle, L. 1995, AJ, 109, 2757
Nomoto, K., Kobayashi, C., & Tominaga, N. 2013, ARA&A, 51, 457
Nomoto, K., Maeda, K., Umeda, H., & Nakamura, T. 2001, in Astrophysics and Space Science Library, Vol. 264, The Influence of Binaries on Stellar Population Studies, ed. D. Vanbeveren, 507
Qian, Y. Z. & Wasserburg, G. J. 2001, ApJ, 549, 337
Qian, Y. Z. & Wasserburg, G. J. 2007, Phys. Rep., 442, 237
Roederer, I. U., Preston, G. W., Thompson, I. B., et al. 2014, AJ, 147, 136
Sbordone, L., Caffau, E., Bonifacio, P., & Duffau, S. 2014, A&A, 564, A109
Schlafly, E. F. & Finkbeiner, D. P. 2011, ApJ, 737, 103
Skúladóttir, Á. & Salvadori, S. 2020, A&A, 634, L2
Skúladóttir, Á., Tolstoy, E., Salvadori, S., Hill, V., & Pettini, M. 2017, A&A, 606, A71
Sneden, C., Cowan, J. J., & Gallino, R. 2008, ARA&A, 46, 241
Spite, F., Spite, M., Barbuy, B., et al. 2018, A&A, 611, A30
Umeda, H. & Nomoto, K. 2002, ApJ, 565, 385
Watson, D., Hansen, C. J., Selsing, J., et al. 2019, Nature, 574, 497